Kinetic, Mechanistic, and Structural Aspects of Unliganded Gating of Acetylcholine Receptor Channels

A Single-channel Study of Second Transmembrane Segment 12′ Mutants

Claudio Grosman and Anthony Auerbach

From the Department of Physiology and Biophysics, State University of New York at Buffalo, Buffalo, New York 14214

abstract The spontaneous activity of adult mouse muscle acetylcholine receptor channels, transiently expressed in HEK-293 cells, was studied with the patch-clamp technique. To increase the frequency of unliganded openings, mutations at the 12′ position of the second transmembrane segment were engineered. Our results indicate that: (a) in both wild type and mutants, a C ↔ O kinetic scheme provides a good description of spontaneous gating. In the case of some mutant constructs, however, additional states were needed to improve the fit to the data. Similar additional states were also needed in one of six patches containing wild-type acetylcholine receptor channels; (b) the δ12′ residue makes a more pronounced contribution to unliganded gating than the homologous residues of the α, β, and ϵ subunits; (c) combinations of second transmembrane segment 12′ mutations in the four different subunits appear to have cumulative effects; (d) the volume of the side chain at δ12′ is relevant because residues larger than the wild-type Ser increase spontaneous gating; (e) the voltage dependence of the unliganded gating equilibrium constant is the same as that of diliganded gating, but the voltage dependences of the opening and closing rate constants are opposite (this indicates that the reaction pathway connecting the closed and open states of the receptor changes upon ligation); (f) engineering binding-site mutations that decrease diliganded gating (αY93F, αY190W, and αD200N) reduces spontaneous activity as well (this suggests that even in the absence of ligand the opening of the channel is accompanied by a conformational change at the binding sites); and (g) the diliganded gating equilibrium constant is also increased by the 12′ mutations. Such increase is independent of the particular ligand used as the agonist, which suggests that these mutations affect mostly the isomerization step, having little, if any, effect on the ligand-affinity ratio.

key words: nicotinic receptors • allosteric proteins • site-directed mutagenesis

INTRODUCTION

The acetylcholine receptor channel (AChR)[1] is a synaptic receptor ion channel (Karlin and Akabas, 1995) whose activation can be understood in the framework of thermodynamic cycles with spontaneous gating and two ligand-binding events as the elementary steps (Monod et al., 1965; Jackson, 1989; Edelstein and Changeux, 1998). Accordingly, the equilibrium properties of unliganded gating determine those of liganded gating. For example, a recombinant AChR engineered to have a more favorable spontaneous opening reaction will also have a higher tendency to be open when diliganded.

In wild-type AChRs, as in any other allosteric protein, the gating equilibrium constant of the unliganded receptor is finely tuned to ensure the appropriate response both in the presence and absence of the ligand (Jackson, 1989). Mutations that increase the gating equilibrium constant of unliganded AChRs have been shown to cause disease (Zhou et al., 1999a). It is thus of considerable importance to investigate the molecular mechanisms of unliganded gating.

There have been only a few studies of AChR spontaneous gating (Brehm et al., 1984; Jackson, 1984, 1986; Jackson et al., 1990). In wild-type receptors, the paucity and brevity of unliganded openings make the characterization of this activity difficult. In addition, in cultured muscle cells, the precise molecular identity of the AChRs under study is not known with certainty because the presence of receptors having unusual subunit stoichiometries, in patches usually containing thousands of channels (Jackson, 1986), is almost impossible to rule out. AChRs formed with only the α, β, and δ subunits exhibit more frequent spontaneous openings than complete $\alpha_2\beta\delta\epsilon$ receptors, but their respective mean open life times and single-channel conductances are indistinguishable (Jackson et al., 1990; Zhou et al., 1999b). Therefore, the extent to which these defective channels contribute to the "wild-type" unliganded activity remains an unsolved issue. This is, however, less of a concern

Address correspondence to Claudio Grosman, Department of Physiology and Biophysics, School of Medicine and Biomedical Sciences, SUNY at Buffalo, 124 Sherman Hall, Buffalo, NY, 14214. Fax: 716-829-2569; E-mail: grosman@buffalo.edu

[1]*Abbreviations used in this paper:* AChR, acetylcholine receptor channel; M2, second transmembrane segment.

J. Gen. Physiol. © The Rockefeller University Press • 0022-1295/2000/05/621/15 $5.00
Volume 115 May 2000 621–635
http://www.jgp.org/cgi/content/full/115/5/621

when dealing with recombinant receptors expressed in HEK-293 cells, the system used in this paper. The small number of AChRs per patch makes the identification of ϵ/γ-less receptors, in the presence of ACh and at the single-channel level, unequivocal (Zhou et al., 1999b).

The frequency of unliganded openings has been shown to increase as a result of several different mutations, most notably in the second transmembrane segment (M2) (Ohno et al., 1995; Auerbach et al., 1996; Engel et al., 1996; Milone et al., 1997). Thus, we decided to study M2-mutant AChRs as a means of magnifying this otherwise almost intractable aspect of the channel's function. We chose the 12′ position (a Ser in δ, and Thr in α, β, and ϵ), which is near the middle of the M2 segment, for three reasons. First, it was known that a mutation at this position of the ϵ subunit increases spontaneous activity (Ohno et al., 1995; Auerbach et al., 1996). Second, this position is one of the very few M2 positions conserved among the entire superfamily of nicotinoid receptors (Table I). Finally, two naturally occurring mutations at this position have been shown to cause a slow-channel congenital myasthenic syndrome (α12′ T→I, Croxen et al., 1997; ϵ12′ T→P, Ohno et al., 1995). Cysteine-scanning mutagenesis studies suggested that the 12′ residues of the α and β subunits do not face the channel conduction pathway (Akabas et al., 1994; Zhang and Karlin, 1998), while affinity-labeling experiments with snake α-neurotoxins suggested that, in *Torpedo*, δ12′ is accessible from the extracellular side (Machold et al., 1995a).

Here, we show that the unliganded activity of M2 12′ mutants largely resembles that of AChRs from embryonic cultured mouse muscle (Jackson, 1984, 1986). The higher frequency of the mutants' spontaneous openings allowed us to extend our understanding of this phenomenon by addressing issues that bear not only on the kinetics but also on the structural and mechanistic aspects of unliganded gating.

METHODS

Mutagenesis and Expression

Mouse cDNA clones were generously provided by Dr. S.M. Sine (Department of Physiology and Biophysics, Mayo Foundation, Rochester, MN), who had obtained them from the late Dr. J. Merlie and Dr. N. Davidson (α, β, and δ subunits), and Dr. P. Gardner (ϵ subunit, Gardner, 1990), in the CMV-based expression vector pRBG4 (Lee et al., 1991; Sine, 1993). The α subunit had a background mutation in M4 (V433A), which does not significantly affect the gating behavior of diliganded AChRs (Salamone et al., 1999). ϵT264P, αY93F, αY190W, and αD200N cDNAs in pRBG4 were generously provided by Dr. Sine. Mutations αT254S, βT265S, δS268A, δS268C, δS268I, δS268N, and δS268Y were engineered using the QuikChange™ Site-Directed Mutagenesis Kit (Stratagene Inc.) protocol. Mutations αT254P, βT265P, δS268P (Chen and Auerbach, 1998), δS268T, and ϵT265S were engineered by overlap PCR (Higuchi, 1990). All constructs were confirmed by dideoxy sequencing.

Human embryonic kidney fibroblast cells (HEK 293) were transiently transfected using calcium phosphate precipitation (Ausubel et al., 1992). A total of 3.5 μg of cDNA per 35-mm culture dish in the ratio 2:1:1:1 (α:β:δ:ϵ) was applied to the cells for ~20 h, after which the medium was changed. Electrophysiological recordings started ~30 h later.

Patch-Clamp Recordings

Recordings were performed in the cell-attached patch configuration (Hamill et al., 1981) at ~22°C. The bath solution was Dulbecco's phosphate-buffered saline containing (mM): 137 NaCl, 0.9 $CaCl_2$, 2.7 KCl, 1.5 KH_2PO_4, 0.5 $MgCl_2$, and 8.1 Na_2HPO_4, pH 7.3. The pipette solution contained (mM): 142 KCl, 5.4 NaCl, 1.8 $CaCl_2$, 1.7 $MgCl_2$, 10 HEPES/KOH, pH 7.4. Patch pipettes pulled from borosilicate capillaries were coated with Sylgard (Dow Corning Corp.) and fire-polished. Pipette resistances ranged between 7.5 and 12.5 MΩ. Pipettes outside this range were discarded in an attempt to exert some control on the area of patched membrane. Unless otherwise stated, the potential of the patch pipette was held at +65 mV, which corresponds to an estimated membrane potential of approximately −100 mV. The membrane potential was estimated based on the amplitude of the single-channel currents and the single-channel conductance. Single-channel currents were recorded using an Axopatch 200B (Axon Instruments) at a 100-kHz bandwidth, digitized at a frequency of 94.4 kHz (VR-10B, f_c = 37 kHz; Instrutech Corp.), and stored on videotape. For analysis, the recordings were transferred to a PC via a digital interface (VR111; Instrutech Corp.) at a sampling frequency of 94.4 kHz.

Some of the mutants studied exhibited high levels of spontaneous activity, but some of them did not. For the latter, it was critical to distinguish between low activity and low expression levels. Rather than relying on the expression of a reporter gene, we identified AChR-expressing cells by making seals, with 5-μM ACh in the pipette, on cells having the typical morphological alterations of cells that are expressing the transfected DNA. Only those cells displaying activity in the presence of ACh were further patched using another pipette that did not contain ACh. In some cases, series of up to six seals on the same cell, alternating the presence and the absence of the agonist, were performed. Only those series displaying activity whenever ACh was present in the pipette were considered for analysis. To prevent contamination of ACh-free solutions with ACh, the pipette electrode (i.e., the Ag/AgCl wire connected to the headstage) was extensively washed with distilled water after each time it came in contact with the agonist. Separate filling needles were used throughout.

Data Analysis

The QUB suite of programs was used (www.qub.buffalo.edu). Single-channel recordings were inspected visually (program PRE) and segmented into ~1.5-s–long stretches of data. Noisy sections and those containing simultaneous openings of two or more channels were excluded. Typically, >98% of the original recording was retained for the kinetic analysis. The data were further filtered digitally (Gaussian filter; effective bandwidth: ~18 kHz) and idealized (program SKM) by using a hidden-Markov modeling procedure (recursive Viterbi algorithm) known as the "segmental k-means" method (Rabiner et al., 1986). Current amplitudes were also estimated during this idealization process.

The list of dwell times generated with SKM was used to obtain kinetic parameters in two different ways. One method consisted of estimating the mean duration of detected closures and openings (here referred to as τ_c and τ_o, respectively) by averaging the corresponding idealized dwell times. This calculation is what a maximum likelihood approach would perform when applied to a

TABLE I

M2 Sequence Alignment of the Members of the Superfamily of Nicotinoid Receptors

Subunit	1′	2′	3′	4′	5′	6′	7′	8′	9′	10′	11′	**12′**	13′	14′	15′	16′	17′	18′	19′
m/hAChRα	M	T	L	S	I	S	V	L	L	S	L	**T**	V	F	L	L	V	I	V
tAChRα	M	T	L	S	I	S	V	L	L	S	L	**T**	V	F	L	L	V	I	V
m/hAChRβ	M	G	L	S	I	F	A	L	L	T	L	**T**	V	F	L	L	L	L	A
tAChRβ	M	S	L	S	I	S	A	L	L	A	V	**T**	V	F	L	L	L	L	A
m/hAChRδ	T	S	V	A	I	S	V	L	L	A	Q	**S**	V	F	L	L	L	I	S
tAChRδ	M	S	T	A	I	S	V	L	L	A	Q	**A**	V	F	L	L	L	T	S
m/hAChRγ	C	T	V	A	T/I	N	V	L	L	A	Q	**T**	V	F	L	F	L	V/L	A
tAChRγ	C	T	L	S	I	S	V	L	L	A	Q	**T**	I	F	L	F	L	I	A
m/hAChRϵ	C	T	V	S	I	N	V	L	L	A	Q	**T**	V	F	L	F	L	I	A
hAChRα2	I	T	L	C	I	S	V	L	L	S	L	**T**	V	F	L	L	L	I	T
hAChRα3	V	T	L	C	I	S	V	L	L	S	L	**T**	V	F	L	L	V	I	T
hAChRα4	I	T	L	C	I	S	V	L	L	S	L	**T**	V	F	L	L	L	I	T
hAChRα5	I	C	L	C	T	S	V	L	V	S	L	**T**	V	F	L	L	V	I	E
hAChRα6	V	T	L	C	I	S	V	L	L	S	L	**T**	V	F	L	L	V	I	T
hAChRα7	I	S	L	G	I	T	V	L	L	S	L	**T**	V	F	M	L	L	V	A
chAChRα8	I	S	L	G	I	T	V	L	L	S	L	**T**	V	F	M	L	L	V	A
hAChRα9	V	S	L	G	V	T	I	L	L	A	M	**T**	V	F	Q	L	M	V	A
hAChRβ2	M	T	L	C	I	S	V	L	L	A	L	**T**	V	F	L	L	L	I	S
hAChRβ3	L	S	L	S	T	S	V	L	V	S	L	**T**	V	F	L	L	V	I	E
hAChRβ4	M	T	L	C	I	S	V	L	L	A	L	**T**	F	F	L	L	L	I	S
h5-HT_{3A}	V	S	F	K	I	T	L	L	L	G	Y	**S**	V	F	L	I	I	V	S
h5-HT_{3B}	I	V	F	K	T	S	V	L	V	G	Y	**T**	V	F	R	V	N	M	S
m/hGlyRα1-4	V	G/A	L	G	I	T	T	V	L	T	M	**T**	T	Q	S	S	G	S	R
hGlyRβ	V	P	L	G	I	F	S	V	L	S	L	**A**	S	E	C	T	T	L	A
$hGABA_A$α1-6	T	V	F	G	V/I	T	T	V	L	T	M	**T**	T	L	S	I	S	A	R
$hGABA_A$β1-3	V	A	L	G	I	T	T	V	L	T	M	**T**	T	I	S/N	T	H	L	R
r/$hGABA_A$γ1-3	T	S/A/T	L	G	I	T	T	V	L	T	M	**T**	T	L	S	T	I	A	R
$hGABA_A$δ	V	S	L	G	I	T	T	V	L	T	M	**T**	T	L	M	V	S	A	R
$hGABA_A$ϵ	T	S	L	G	I	T	S	V	L	T	M	**T**	T	L	G	T	F	S	R
$hGABA_A$π	T	C	I	G	V	T	T	V	L	S	M	**T**	T	L	M	I	G	S	R
$hGABA_C$ρ1	V	P	L	G	I	T	T	V	L	T	M	**S**	T	I	I	T	G	V	N
$hGABA_C$ρ2	V	S	L	G	I	T	T	V	L	T	M	**T**	T	I	I	T	G	V	N

M2 residues are usually referred to by following a numbering system that ranges from 1′ at the intracellular end to 19′ at the extracellular one. Residues occupying the 12′ position are bolded. The sequences of all subunits were taken from the SWISS-PROT Protein Sequence Database with the exception of AChRα8 (Schoepfer et al., 1990) and 5-HT_{3B} (Davies et al., 1999). Whenever possible, the human (h) sequences are given; otherwise, the sequences of either chicken (ch), mouse (m), or rat (r) are indicated. The M2 sequences of the human α, β, δ, and ϵ AChR subunits are identical with those of mouse (the clones used in this paper). *Torpedo* (t) sequences are also included.

two-state, C ↔ O model without correction for missed events. The reciprocal of τ_c was taken as an estimate of the opening frequency which, as long as openings are brief, is a good approximation. Because the number of channels in the patch was not known, this parameter is a measure of both the opening frequency per channel and the number of channels in the patch. The open probability was calculated as $\tau_o/(\tau_o + \tau_c)$ and, because it is not a measure of the single-channel open probability, we refer to it as "patch open probability". The second procedure (program MIL; Qin et al., 1996, 1997) was used for kinetic modeling of the dwell-time series to find the model and rate constants that fit the data best. It consists of an interval-based full-likelihood algorithm (Horn and Lange, 1983; Chay, 1988) that includes a correction for missed events based on a first-order approximation (Roux and Sauvé, 1985). A fixed resolution was imposed on the open and closed times (the same for both) by considering all dwell times shorter than a given value ("dead time") as belonging to the conductance of the flanking sojourns. The average dead time was 26 μs and in most cases it was 18 μs. Standard errors of the rate-constant estimates were calculated from the curvature (second derivative) of the likelihood surface at its maximum.

In the case of currents elicited by saturating concentrations of choline (20 mM) or acetylthiocholine (2 mM), clusters of single-channel openings were defined as a series of openings separated by closures shorter than a critical time (τ_{crit}). For every patch, different τ_{crit} values were tested and the corresponding idealized intracluster dwell-time series were analyzed with MIL (f_c = 18 kHz; dead time ≅ 30 μs). Because diliganded gating is very likely to proceed from a single closed diliganded state, the longest τ_{crit} defining clusters whose kinetics of closed durations were still best modeled by a single closed state was chosen. To discriminate between models with one or two closed states, we compared the corresponding maximum log-likelihood values. The two extra free parameters of the model with two closed states were penalized by subtracting two units from its maximum log-likelihood value (asymptotic information criterion; Korn and Horn, 1991). The mean

open time of each cluster was calculated and compared with those of the other clusters in the same patch. Only those clusters whose mean open times were within ±2 SD of the overall mean of the corresponding patch were retained for further analysis.

RESULTS

In the absence of ligand, wild-type AChRs open rarely and briefly. Fig. 1 shows a continuous stretch of data illustrating the spontaneous activity of recombinant, adult muscle AChRs transiently expressed in HEK-293 cells. Some kinetic parameters are listed (see Tables II and IV).

Fig. 2 illustrates the effect of the M2 12′ δS→T mutation at the single-channel level. Both the frequency and average duration of spontaneous openings are considerably increased by the mutation. In four of five patches, multiple closed and open components were apparent, with the longest (and least frequent) type of openings occurring in bursts. However, in all patches, short-lived isolated openings accounted for the majority of events. Estimates of the opening frequency, mean duration of detected openings (τ_o), and patch open probability are displayed in Table II.

We next tested the effect of T→S single mutations in the 12′ positions of the other subunits. The results in Table II suggest that T→S substitutions in the β or ϵ subunit exert little (if any) effect, while this mutation in both α subunits decreases the spontaneous activity of the wild type to undetectable levels. We then expressed combinations of mutant subunits to generate AChRs that, like the wild type, have a Ser in only one type of subunit. As expected from mutational effects that are cumulative (if not additive; Wells, 1990), double-mutant AChRs having a single S in β or ϵ display high spontaneous activity, comparable with the sum of the effects of the single mutants. Likewise, adding the T→S mutation in both α subunits to δS→T receptors reduces unliganded activity, as it does when added to the wild type. We conclude that the residues occupying the 12′ position of the different subunits make asymmetric contributions to unliganded activity, the δ subunit playing the most prominent role. Also, since the mutational effects do not seem to deviate from additivity, we conclude that the five subunits are likely to make independent contributions to gating.

Estimates of opening frequency, mean duration of detected openings, and patch open probability of different δ12′ mutants and of the Pro mutants in the four subunits are also listed in Table II. The very large "opening frequency" of α12′ T→P receptors resulted, at least in part, from an increased number of openings per burst, as analyzed below.

A Kinetic Model

The parameters in Table II do not fully reflect the differences between the spontaneous activity of wild-type and mutant receptors that are clear from even a cursory examination of the recordings. Particularly, the multiplicity of open states is not represented at all in Table II, where all open durations were averaged into a single value. We therefore sought to characterize the behavior of unliganded gating in terms of rate constants. It is worth noting that the occurrence of bursts of openings was not always observed. In the δS→T mutant, these bursts were recorded in four of five patches, while in the wild type they were detected in only one of six patches, even with cells corresponding to the same transfection batch. The other constructs, however, displayed this component in either all, or none, of the patches. The kinetic analysis below was performed on single-channel records from patches that exhibited these bursts. With the exception of noisy sections and those containing simultaneous openings of two or more channels, which typically represented <2% of the original data, the recordings were analyzed in their entirety.

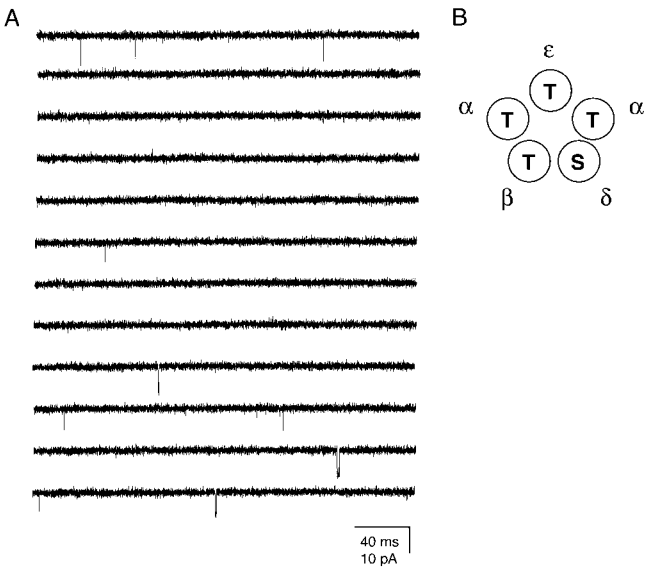

Figure 1. Wild-type unliganded gating. (A) Continuous single-channel traces of spontaneous openings recorded at an estimated membrane potential of −120 mV. For display purposes, $f_c \cong 6$ kHz. Openings are downward deflections. (B) Schematic representation of the residues occupying the M2 12′ position in wild-type receptors. The ordering of the subunits, as seen from the extracellular side, is as suggested by Machold et al. (1995b).

What follows is an example of model discrimination applied to a particular dwell-time sequence (4,226 events) obtained from a patch of a cell expressing the δS→T mutant. Fig. 3 shows all the kinetic models tested, and Table III displays the corresponding maximum likelihood values expressed as log-likelihood ratios (LLR*exp*), taking A as the reference (i.e., maximum log-likelihood value for model *i* – maximum log-likelihood value for A, where model *i* is any model from B to J). A comparison of the LLR*exp* values leads to the re-

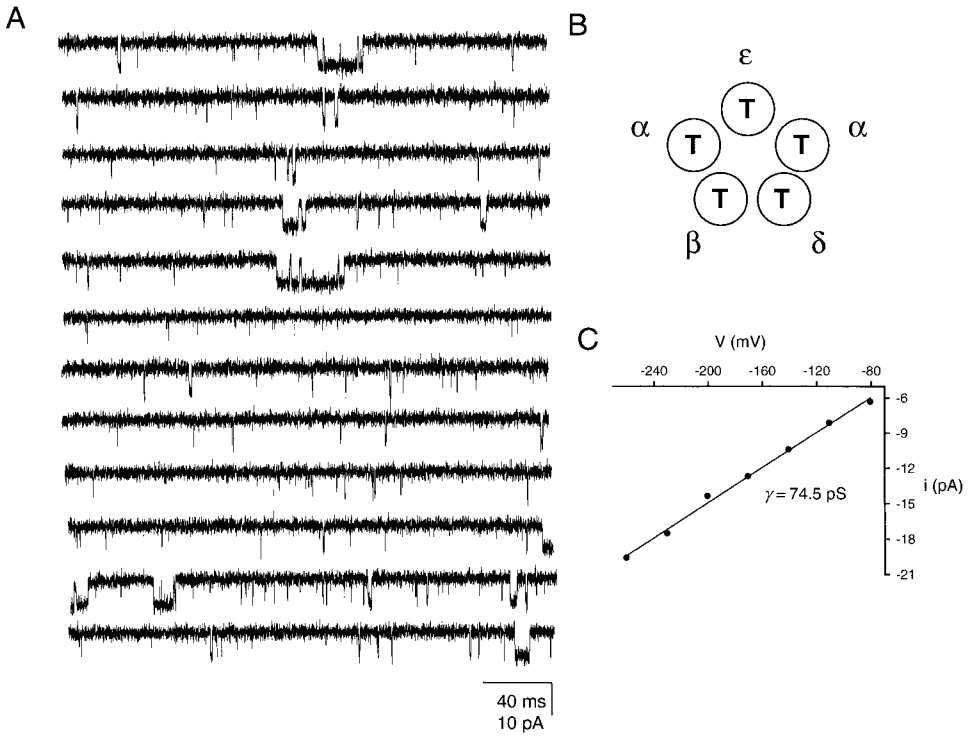

Figure 2. δS→T AChR unliganded gating. (A) Continuous single-channel traces of spontaneous openings recorded at approximately −100 mV. Note the multiplicity of closed- and open-time components. Display $f_c \cong 6$ kHz. Openings are downwards. (B) Schematic representation of the residues occupying the M2 12′ position in δS→T receptors. (C) I-V curve under cell-attached conditions and least-square fit with a straight line.

jection of B, D, and E, which suggests that at least two closed and three open states are needed to describe the kinetics of the data, and that the second closed state has to be connected to one of the open states (compare A and E). Sojourns in this additional closed state (C_4) account for the population of brief closures present within bursts of openings. The best fit to the data always connected this short-lived closed state to the slowest open state (with the exception of the αT→P mutant), in agreement with the observation that openings

TABLE II

Kinetic Properties of Unliganded Gating in M2 12′ Mutants

AChR	12′ residue α	β	δ	ϵ	Opening frequency	τ_o	P_o	*n*
					s^{-1}	*ms*		
Wild type	T	T	S	T	1.46	0.209	3.02×10^{-4}	6
δS268T	T	T	T	T	23.85	0.555	1.45×10^{-2}	5
ϵT264S	T	T	S	S	1.41	0.081	1.11×10^{-4}	4
βT265S	T	S	S	T	5.23	0.143	7.48×10^{-4}	1
αT254S	S	T	S	T	*	*	*	>10
δS268T + ϵT264S	T	T	T	S	15.86	0.984	1.51×10^{-2}	4
δS268T + βT265S	T	S	T	T	24.40	1.120	2.68×10^{-2}	3
δS268T + αT254S	S	T	T	T	5.00	0.054	2.51×10^{-4}	3
δS268A	T	T	A	T	8.73	0.405	3.45×10^{-3}	2
δS268C	T	T	C	T	1.98	0.111	2.62×10^{-4}	4
δS268N	T	T	N	T	6.02	1.46	8.78×10^{-3}	1
δS268I	T	T	I	T	6.77	0.672	4.55×10^{-3}	1
δS268Y	T	T	Y	T	6.11	0.802	5.86×10^{-3}	2
δS268P	T	T	P	T	14.80	0.594	8.23×10^{-3}	3
βT265P	T	P	S	T	12.20	1.162	1.29×10^{-2}	2
ϵT264P	T	T	S	P	9.59	0.454	3.58×10^{-3}	2
αT254P	P	T	S	T	137.41	0.108	1.20×10^{-2}	2

The displayed values of unliganded opening frequency, mean duration of detected openings (τ_o), and patch open probability (P_o) are the corresponding mean values for the indicated number of patches (*n*). *No openings were detected.

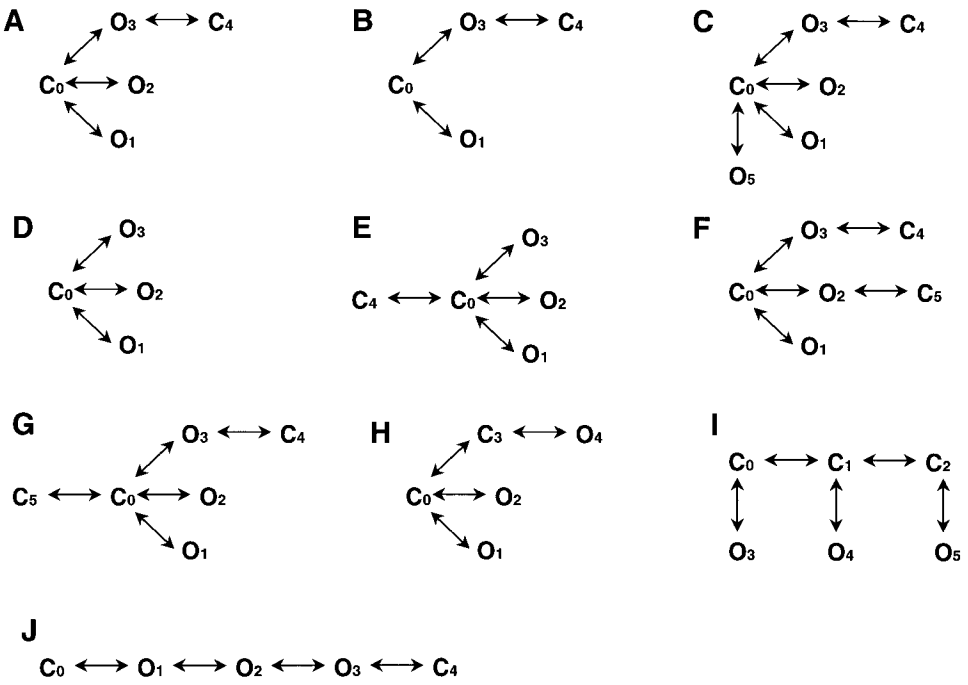

Figure 3. Set of reaction schemes used for kinetic modeling according to a full-likelihood approach. C, nonconductive; O, open. Whether these models represent different closed–open transitions of individual receptors or the gating activity of heterogeneous receptors in the patch is not known.

within a burst are longer than isolated openings. Both A and H satisfy these conditions and LLR*exp* = 0. C and F were rejected because the rates leading to O_5 (C) and C_6 (F) were negligibly small and, therefore, sojourns in these states are very rare.

Throughout this procedure, only large LLR values were taken into account to discriminate between models and, thus, application of penalties for excess free-parameters did not affect the decisions. The LLR*exp* values and rate constants corresponding to Fig. 3, G, I, and J, however, did not allow a clear decision to be made. Therefore, we simulated noise-free single-channel event lists (containing approximately the same number of events as the original data) according to each model in Fig. 3. Analysis of the simulated data (Table III) and comparison with the LLR*exp* values confirms that G, I, and J cannot be ruled out as appropriate kinetic schemes for spontaneous gating.

We conclude that, for the δ S→T mutant, A, G, H, I, and J in Fig. 3 are all plausible, with A, H, I (constrained), and J being the most parsimonious. Simulating dwell-time sequences containing ~10× more intervals revealed that I (constrained) and J could have been distinguished from A and H if more data had been collected. As expected, however, A and H could not have.

The maximum log-likelihood value obtained with Fig. 3 A was then compared with that obtained from fitting the experimental data to a fully connected model with the same number of closed and open states. In such a model, all connections between states (regardless of their conductances) are allowed, the corresponding maximum-likelihood value being the highest possible for

TABLE III

LLR-based Discrimination among Kinetic Models of Unliganded Gating for δS→T AChRs

Model	LLR*exp*	LLR*i*	LLR*A*
B	−48	0	−25
C	+6	+7	+7
D	−141	+2	−134
E	−114	+36	−121
F	+2	+2	0
G	+2	+4	+3
H	0	+7	+4
I (unconstrained)	+2	+11	+5
I (constrained)*	−2	+9	+1
J	−11	+1	−3

Example of model discrimination applied to a particular dwell-time series of the 12′ δS→T mutant (patch 1). Log-likelihood ratio values (LLR) between *i* (B to J) and A (Fig. 3) were computed from the experimental data (LLR*exp*) and from simulated data (program SIMU, QUB suite) according to *i* (LLR*i*) or A (LLR*A*). A dead time of 18 μs was used throughout. The rate constants used for simulation were the rate-constant estimates obtained by maximum-likelihood fitting of the experimentally derived dwell-time series to either model. If the models made very different predictions, LLR*i* would be a positive number, whereas LLR*A* would be a negative number (because LLR values are calculated with A as reference). Assuming that the variables LLR*i* and LLR*A* are normally (Gaussian) distributed and that their standard deviations are similar, comparison of the LLR*i* and LLR*A* values in any given row with the corresponding LLR*exp* should lead to a decision (Korn and Horn, 1991). Only one dwell-time sequence per model was simulated and used for the calculation of the LLR*i* and LLR*A* values. *k_{01} was constrained to be twice k_{12}, and k_{21} was constrained to be twice k_{10} (Fig. 3), as if two equivalent conformational rearrangements separated C_0 from C_2.

the given number of closed and open states (for a related approach, see Rothberg and Magleby, 1998). The LLR between these two models was zero, indicating that no other model with two closed and three open states can describe the data better. The rate-constant estimates to A for this example patch (No. 1) are shown in Table IV for comparison with other mutants, and in Table V for comparison with three other δS→T patches (Nos. 2–4) where the three types of openings were present. A model discrimination analysis of these three other patches supports all the conclusions above for patch No. 1.

A similar procedure was applied to all other constructs that exhibited multiple open and closed components. Fig. 4 shows the dwell-time histograms and the superimposed density functions of example patches, and Table IV shows the corresponding rate constants. The kinetics of the δS→T + βT→S and εT→P constructs, like those of the δS→T mutant, were best described by Fig. 3, A, G, H, I, and J. The corresponding rate-constant estimates to A are shown in Table IV. For the wild type and the mutants δS→T + εT→S, δS→A, δS→N, δS→I, δS→P, and βT→P, Fig. 3 B (with only two open states) was superior. In these seven cases, the intermediate open state was of doubtful existence, a fact that could be related to its lifetime being close to (and thus difficult to distinguish from) that of either the fastest or slowest type of openings, rather than to a genuine mechanistic difference between mutants. Finally, the mutants δS→Y and αT→P were fitted best to G. Again, we think that this difference may reflect some data heterogeneity rather than a different gating mechanism. For any given mutant, the rank order of the models was the same for all patches.

Other than the opening rates, which in our case depended on the number of channels in the patch, the rate constants varied little between constructs. However, two noteworthy differences were present. First, δS→A and wild-type AChRs have larger k_{30} values, which make their longest-lived openings shorter than those of the other mutants (Fig. 5). Nevertheless, as k_{34} values are also increased, these openings still occur in bursts with a "regular" number of openings. Second, αT→P AChRs have a much larger k_{34}, which greatly increases the number of openings per burst and reduces the duration of these openings to as little as ∼150 μs (Fig. 5). If, for example, Fig. 3 H were used instead (where the bursting behavior is modeled by a C ↔ C→O scheme), an increase in two rate constants, k_{43} and k_{34}, would be needed to account for the same finding.

If we assume that the multiple kinetic components arise from the activity of individual channels, then, in bursty patches, the unliganded AChR can access three different open conformations with mean lifetimes of ∼100 μs (>75% of the total openings), ∼500 μs, and ∼5 ms. From the rate-constant estimates, it can be calculated that the longest openings are grouped in bursts of, on average (and excluding the αT→P mutant), ∼1.29 openings separated by brief (∼150 μs) gaps. In other words, ∼60% of these openings occur as isolated events, ∼27% occur as pairs of openings separated by a brief gap, ∼9%

TABLE IV

Kinetic Modeling of Unliganded Gating in M2 12′ Mutants

AChR	Rates								Openings per burst*	$n^{‡}$	Kinetic model
	k_{01}	k_{10}	k_{02}	k_{20}	k_{03}	k_{30}	k_{34}	k_{43}			
	s^{-1}	s^{-1}	s^{-1}	s^{-1}	s^{-1}	s^{-1}	s^{-1}	s^{-1}			
Wild type	1.6	10176	—	—	0.7	1112	235.6	13825	1.2	812	B
δS→T	37.5	6547	9.2	1416	2.8	111.8	53.3	2683	1.5	4226	A
δS→T + εT→S	16.0	13102	—	—	1.2	163.4	36.4	4510	1.2	3623	B
δS→T + βT→S	11.1	11590	3.3	3266	1.2	95.8	43.6	1843	1.5	928	A
δS→A	4.1	4484	—	—	1.1	1006	102.9	8497	1.1	2085	B
δS→N	5.4	6533	—	—	0.5	72.6	55.4	3434	1.8	2742	B
δS→I	5.7	9205	—	—	1.2	356.0	49.4	3034	1.1	2633	B
δS→Y[§]	6.1	13398	4.0	1496	0.9	101.5	35.0	22130	1.3	4752	G
δS→P	9.4	22154	—	—	3.7	701.0	65.6	11419	1.1	969	B
βT→P	6.7	9876	—	—	1.8	185.6	16.8	8141	1.1	1600	B
εT→P	4.1	11325	1.9	3825	0.2	99.1	40.9	1261	1.4	1408	A
αT→P[§]	318.8	32698	0.8	836.1	6.3	859.5	6908	6750	9.0	88242	G

Transition rates were estimated using a full-likelihood algorithm that includes a correction for missed events (program MIL; Qin et al., 1996, 1997). The values in each row correspond to one example patch per construct. The values given here for k_{01}, k_{02}, and k_{03} depend on the number of channels in the patch and are not true rate constants. However, k_{43}, which corresponds to the reopening rate within bursts, and all the closing rates, is a true rate constant. *Calculated as $1 + k_{34}/k_{30}$. ‡Number of shut and open intervals in the idealized dwell-time series after imposing a fixed resolution ("dead time"). §The data were fitted better to G than to A. To allow for a comparison of the opening rates of these two mutants with those of the wild type and the other mutants, the rates indicated here as k_{01}, k_{02}, and k_{03} are values calculated as: $k_{0i}\,k_{50}/(k_{50} + k_{05})$, where i is either 1, 2, or 3 (see Fig. 3 G). These apparent opening rates are the reciprocal of the mean time spent in $C_5 \leftrightarrow C_0$ interconversions weighted by the proportion of openings to O_1, O_2, or O_3.

TABLE V

Patch-to-Patch Variation in the Kinetic-Parameter Estimates of δS→T AChR Unliganded Gating

Patch	Rates								*n*
	k_{01}	k_{10}	k_{02}	k_{20}	k_{03}	k_{30}	k_{34}	k_{43}	
	s^{-1}	s^{-1}	s^{-1}	s^{-1}	s^{-1}	s^{-1}	s^{-1}	s^{-1}	
1	37.5 ± 1.8	6547 ± 335	9.2 ± 1.5	1416 ± 229	2.8 ± 0.4	111.8 ± 13.5	53.3 ± 7.5	2683 ± 436	4226
2	35.2 ± 1.5	6263 ± 217	3.2 ± 1.1	1827 ± 814	1.5 ± 0.5	240.2 ± 46.6	44.0 ± 10.0	2054 ± 1147	6317
3	6.8 ± 0.8	10057 ± 1164	2.9 ± 0.8	2975 ± 460	0.17 ± 0.06	52.7 ± 17.8	19.3 ± 10.8	3254 ± 1874	802
4	5.1 ± 0.7	13267 ± 2244	1.5 ± 0.5	3739 ± 707	0.18 ± 0.07	164.2 ± 66.9	138.8 ± 50.1	1980 ± 822	462

Fig. 3 A was used as the kinetic model. The smaller number of intervals detected in patches 3 and 4 mainly resulted from the slower opening rates k_{01}, k_{02}, and k_{03}. Variation of these values between patches reflects differences in both the opening rate constants and the number of channels in the patch. The total duration of the recordings in the four cases were similar but not equal. Dead times were (μs): 18, 45, 44, and 46 for patches 1–4, respectively. Standard errors were calculated from the curvature of the likelihood surface at its maximum. *n*, number of intervals.

form triplets separated by two gaps, and so on. Fig. 5 shows examples of such bursts for different constructs, including the wild type. In all the cases where multiple open components were not observed, only brief isolated openings, indistinguishable from the fast predominant component described above, were recorded.

The fact that short-lived openings dominated the unliganded activity clearly suggests that these represent the main allosteric transition of wild-type gating. This is the reason why we focused on this kinetic component to study the effects of voltage and binding-site mutations on spontaneous activity (see below). It is not clear, however, what the diliganded counterpart of the longest-lived, less-frequent type of openings is.

Voltage Dependence

It has been known for several decades that the equilibrium constant of AChR-diliganded gating is voltage dependent (Magleby and Stevens, 1972). A reversible cyclic model with only gating and (voltage insensitive) binding steps requires that the voltage dependence of gating be the same regardless of the number of agonists bound to the receptor (0, 1, or 2). The study of the voltage dependence of unliganded gating in recombinant AChRs has been hampered, however, by the low frequency of openings in the case of wild-type AChRs, and by the low expression levels in the case of certain M2 mutants. We therefore explored the voltage dependence of unliganded gating in the 12′ δS→T mutant.

The voltage dependence of the opening and closing rate constants was studied in a patch that displayed only the brief type of openings (i.e., the data were fitted best to a C ↔ O model). The *z*δ parameters were obtained from fits of rate-versus-voltage plots to the Boltzmann equation [$k = k_o \exp(-z\delta F V/RT)$] (Fig. 6). Their values were 0.363 ± 0.024 for the opening and 0.011 ± 0.023 for the closing rate constant. Thus, in this patch, the unliganded gating equilibrium constant increased *e*-fold with an ∼70-mV hyperpolarization, a change that was entirely due to the increase in the opening rate constant. In diliganded AChRs, Auerbach et al. (1996) found that the gating equilibrium constant increases *e*-fold with an ∼66-mV hyperpolarization, but that this change is mainly due to the decrease in the closing rate constant. We conclude that the voltage dependence of the gating equilibrium constant is the same in un- and diliganded gating, but that the voltage dependences of the gating rate constants are opposite.

Effect of Binding-Site Mutations

According to the constraints imposed by a cyclic model with only binding and isomerization steps, unliganded gating must involve a conformational rearrangement in both the pore and the transmitter binding sites, just like during liganded gating. However, the increased spontaneous activity often recorded from recombinant ligand-gated ion channels has been interpreted as arising from the uncoupling of the binding sites from the gate (Auerbach et al., 1996; Neelands et al., 1999). This interpretation implies that, in the absence of ligand, the pore can act autonomously, regardless of the affinity state of the binding sites. In principle, this mechanism of spontaneous gating does not seem unreasonable insofar as most point mutations leading to an increased unliganded activity occur in M2; namely, in the pore domain and ∼50 Å away from the binding sites (Valenzuela et al., 1994; Miyazawa et al., 1999). Moreover, if such a mechanism turned out to be the case, it would be interesting to know to what extent it contributes to the spontaneous activity of wild-type receptors, for which a strictly coupled mechanism has been hypothesized (Jackson, 1989, 1994).

To distinguish between such coupled and uncoupled mechanisms of unliganded gating, we transfected HEK-293 cells with cDNA encoding for 12′ δS→T, 12′ εT→S, β wild type, and either αY93F, αY190W, or αD200N. The combination of both 12′ mutations was shown, above, to yield receptors with high spontaneous activity. The three binding-site mutations in the α subunit have been shown to decrease the diliganded gating equilibrium constant by, mainly, slowing down the channel's opening rate

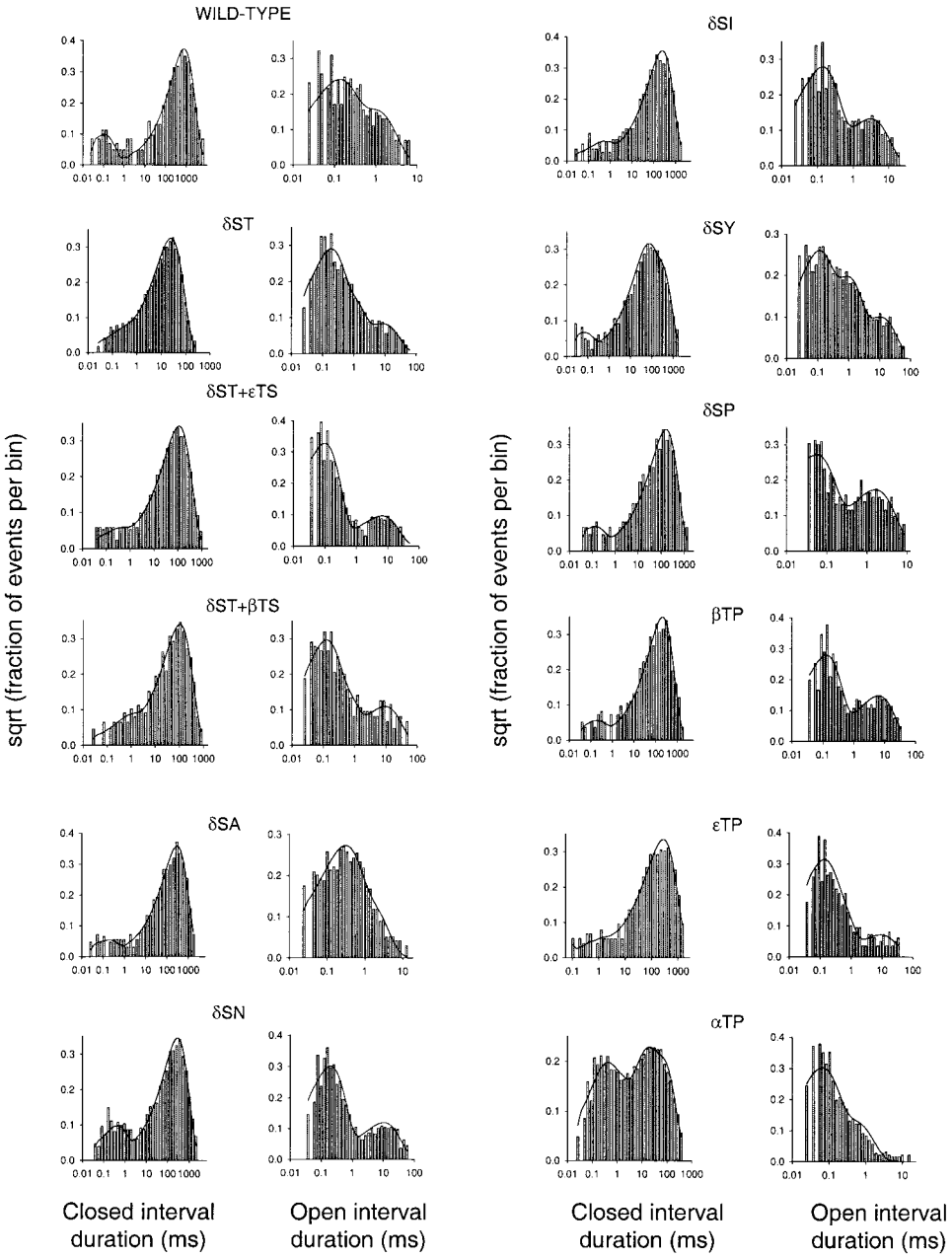

Figure 4. Dwell-time histograms and superimposed density functions corresponding to wild-type and M2 12′ mutant AChR unliganded gating. The kinetics of δS→T, δS→T + βT→S, and ϵT→P receptors were fitted to Fig. 3 A. Those of the wild-type and δS→T + ϵT→S, δS→A, δS→N, δS→I, δS→P, and βT→P receptors were fitted to Fig. 3 B. Those of δS→Y and αT→P receptors were fitted to Fig. 3 G. The corresponding rate constant estimates are listed in Table IV. Each histogram corresponds to data recorded in one example patch for each construct.

(Chen et al., 1995; Akk et al., 1996; Auerbach et al., 1996). We reasoned that if spontaneous activity arose from a local deformation of the pore, then co-expression with the binding-site mutants would have no effect on unliganded activity. Fig. 7 shows that these three binding-site mutations substantially decreased (>15-fold) the frequency of unliganded openings when coexpressed with the 12′ mutations. This suggests that there is a binding-site rearrangement upon unliganded gating.

Diliganded Gating in Channels with Increased Unliganded Activity

The results presented in the above section suggest that both unliganded and diliganded gating result from the same global conformational change, even though, as suggested by the voltage-dependence experiments, the particular pathway followed in each case may differ. This supports the application of thermodynamic cycles to model the AChR's activity, according to which:

$$\theta_2 = \left(\frac{K_d}{J_d}\right)^2 \cdot \theta_0, \qquad (1)$$

where K_d and J_d are the microscopic dissociation equilibrium constants from the closed and open states respectively, and θ_0 and θ_2 are the gating equilibrium constants for the unliganded and diliganded AChR, respectively. Eq. 1 predicts that an increase in θ_0 (caused, for example, by a pore mutation) has to be accompa-

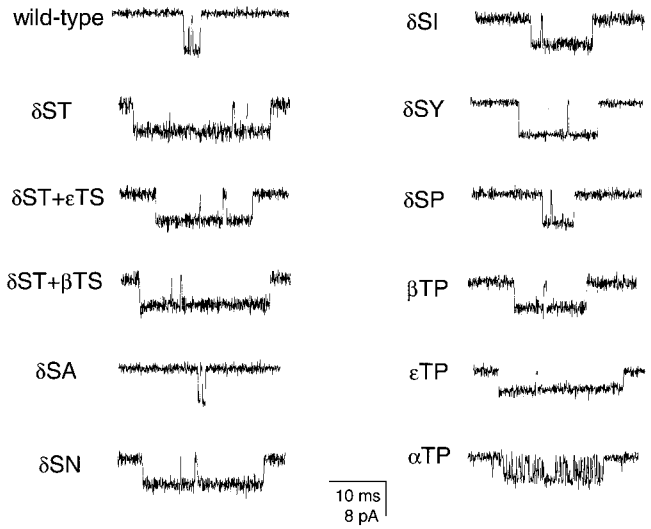

Figure 5. Example bursts of unliganded openings of wild-type and M2 12′ mutant receptors. Display $f_c \cong 6$ kHz. The different current amplitudes most likely reflect differences in the membrane potential. This is most evident in the case of the εT→P mutant, where a somewhat detached patch could have decreased the cell's membrane potential. Openings are downwards.

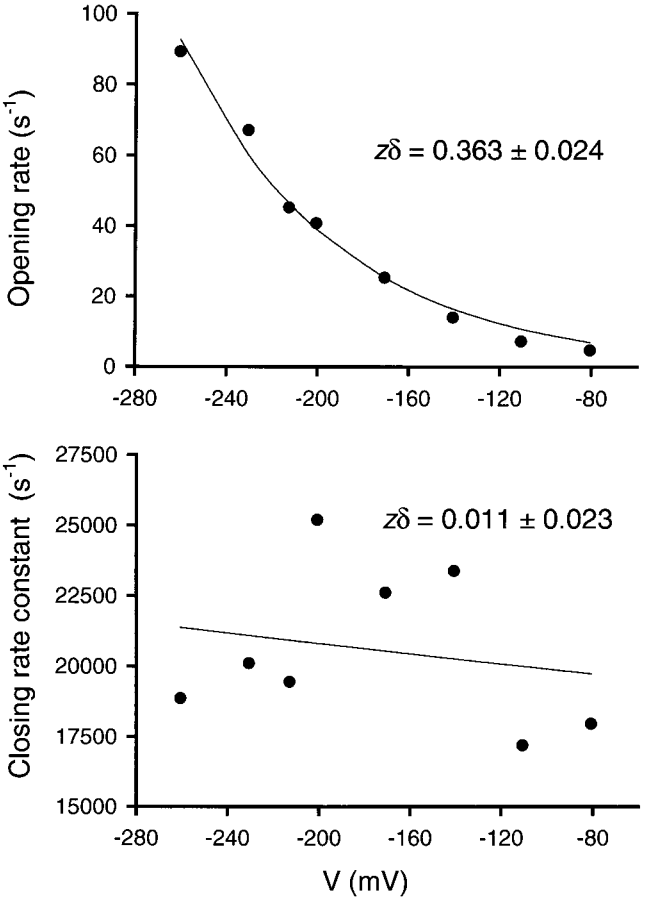

Figure 6. Voltage dependence of 12′ δS→T AChR unliganded gating. Solid lines are fits to the Boltzmann equation for voltage dependence. Because only the brief type of openings was recorded in this patch, the full-likelihood approach was applied to a C ↔ O scheme. The opening rate is assumed to be the product of the opening rate constant and the number of channels in the patch. The particular value of the latter does not affect the zδ estimate.

nied by the same increase in θ_2 as long as the affinity ratio (K_d/J_d) is not affected.

θ_2 values were estimated as the ratio between the opening (β_2) and closing (α_2) rate constants from clusters of single-channel currents elicited at saturating concentrations of agonist (Grosman and Auerbach, 2000). Fig. 8 shows that, in the presence of 2 mM ACh, it is difficult to detect any increase in θ_2 upon the 12′ δS→T mutation. This is because the wild-type's θ_2 value is already near the upper limit of reliable estimation. However, such an increase is readily apparent in the presence of choline or acetylthiocholine (the thioester counterpart of ACh), two slowly opening, low-efficacy agonists (Fig. 8). The δ12′ mutation increases θ_2 by a factor of 14.5 when the AChR is occupied by choline and by a factor of 13.1 when it is occupied by acetylthiocholine (Table VI). The increase in θ_2 thus appears to be independent of the particular agonist used, suggesting that the 12′ δS→T mutation mainly affects θ_0, leaving the K_d/J_d ratio almost unchanged.

DISCUSSION

Kinetic Aspects

In both wild type and M2 12′ mutants, a two-state C ↔ O kinetic scheme provides a good description of spontaneous gating. In the case of some 12′ mutants, however, additional states were needed to improve the fit to the data and similar extra states were needed in one of six patches containing wild-type AChRs. Multiple kinetic components during unliganded gating have also been observed for a number of slow-channel congenital myasthenic syndrome (SCCMS) mutants in M2 (εT264P, Ohno et al., 1995; βV266M and εL269F, Engel et al., 1996; αV249F, Milone et al., 1997), suggesting that these additional kinetic components may be associated with M2 mutations in general. In a few patches of cultured embryonic mouse skeletal muscle, Jackson (1986) described the existence of additional, longer-lived components in the open-time distribution of unliganded gating. Furthermore, heterogeneous kinetics have been reported for liganded gating in both native (Auerbach and Lingle, 1986) and recombinant (Gibb et al., 1990; Naranjo and Brehm, 1993) wild-type AChRs.

There are a number of possible explanations for the multiplicity of kinetic states that we observed during unliganded gating. A trivial explanation is that trace concentrations of ACh (or some other cholinergic ligand) were present and resulted in a small number of liganded openings. We consider this to be unlikely because precautions were taken to avoid such contamina-

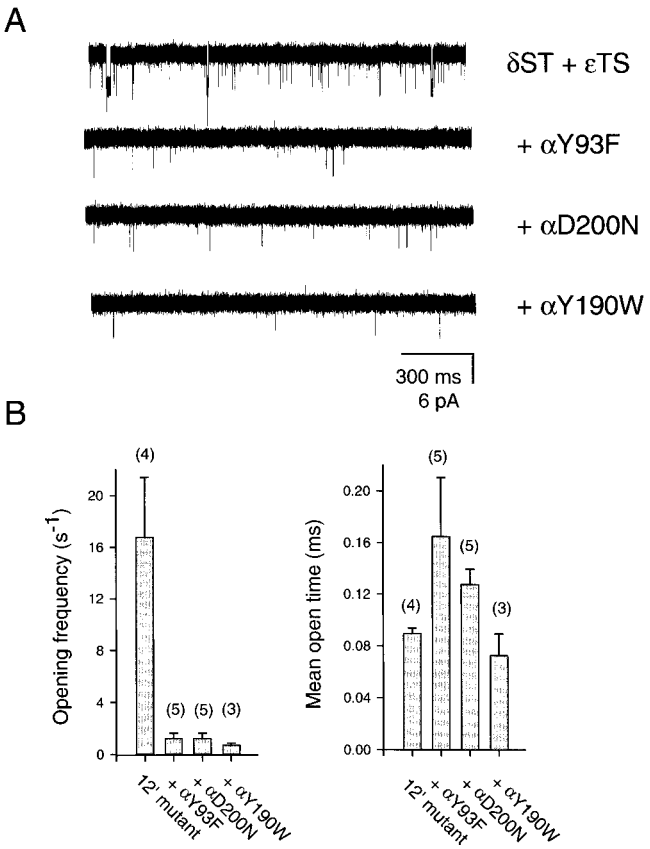

Figure 7. Effect of binding-site mutations on unliganded gating. (A) Representative single-channel traces in the absence of ligand. Display $f_c \cong 6$ kHz. Openings are downwards. The background receptor on which the binding-site mutations were engineered was the double mutant 12′ δS→T + εT→S. (B) Bar representation of opening frequencies, mean open times, and the corresponding standard errors for the four constructs. The number of analyzed patches in each case is indicated in parentheses. The constructs having the binding-site mutations displayed only one type (the briefest one) of openings. However, the kinetics of the 12′ δS→T + εT→S mutant alone were best described by two open states (Fig. 3 B) with mean open times of 89.7 μs (88% of the total openings) and 4.66 ms ($n = 4$). In this case, only the rates associated with the briefest component were considered for comparison with the other three constructs. While the binding-site mutations greatly reduced the frequency of brief openings, little effect was exerted on their mean duration. "Opening frequencies" are the opening rates. Mean open times were calculated as the reciprocal of the closing rate constants, and the corresponding standard errors were calculated using Eqs. 1 and 2 in the companion paper.

tion. A second possibility is that the patches contained a set of heterogeneous receptors. Under our experimental conditions, these could have arisen from alternative assembly patterns and/or different extents of post-translational modifications. However, neither of these are likely to be affected by mutations in δM2 (Verrall and Hall, 1992; Eertmoed and Green, 1999; Swope et al., 1999) and hence the degree of molecular heterogeneity of the mutants studied here is not expected to be any greater than that of recombinant wild-type AChRs. A third clear possibility is that the complex kinetic activity represents an intrinsic property of individual AChRs, which is unveiled by the M2 mutations. The finding that, for some constructs, the complex kinetic behavior was recorded in some, but not all, patches may be attributed to modulation by cellular processes, based on the observation that protein kinase A–catalyzed phosphorylation of *Torpedo* AChRs increases the proportion of long over short unliganded openings (Ferrer-Montiel et al., 1991). In conclusion, although our experiments do not allow us to definitively distinguish between molecular heterogeneity and complex kinetics, the observation that M2 mutations increase the complexity of unliganded gating leads us to suspect that the multiplicity of kinetic states is a property of individual AChRs.

Structural Aspects

Our results suggest that the M2 12′ position of each subunit makes an asymmetric and independent contribution to unliganded gating. We showed that this is also true during diliganded gating (Grosman and Auerbach, 2000). Other mutational studies of the M2 domain also support the idea of an uneven contribution to function made by residues occupying homologous positions in different subunits. This has been shown, in the presence of agonist, for the 2′ (Villarroel et al., 1992), 9′ (Kearney et al., 1996), 12′ (Chen and Auerbach, 1998; Grosman and Auerbach, 2000), and 17′ (Chen and White, 1999) positions. In all these cases, it is the δ subunit that stands out. Whether this reveals differences in the dynamics of the subunits during gating or results from an asymmetric orientation of the five subunits in the pore of the pentameric complex is still unclear.

Voltage Dependence

There is a discrepancy in the literature about the voltage dependence of the unliganded gating rate constants. Although Jackson (1986) showed evidence that the opening rate constant is voltage dependent, the results of Auerbach et al. (1996) suggested that it was not. In the latter case, even though M2 mutations were used to increase spontaneous activity, the observed frequency of openings was so low (<1.5 s^{-1}, presumably due to poor expression levels) that only a few events were usually collected. This limitation could well have been the source of the difference between both reports.

With the 12′ mutants, we were able to record higher frequencies of openings. One remaining problem, however, was that a complex kinetic scheme was generally needed to fit the data. To make the analytic procedure more reliable and the interpretation of the results more straightforward, we analyzed the voltage dependence of unliganded gating in a patch that only displayed the fast class of openings (which, even in the ki-

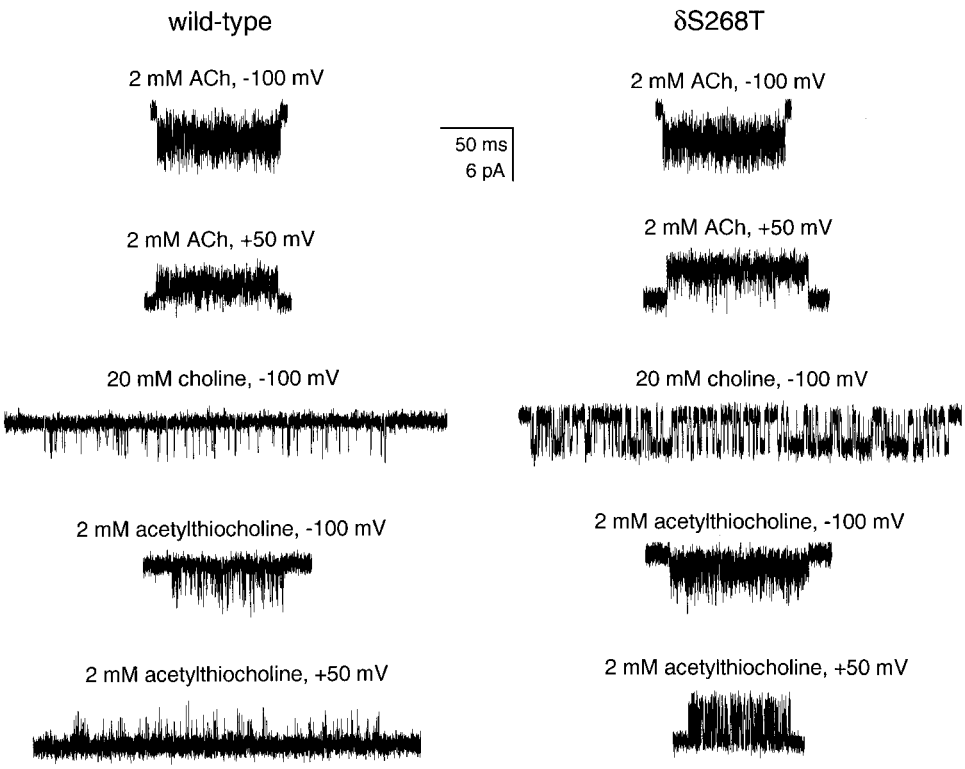

Figure 8. Effect of the 12′ δS→T mutation on diliganded activity. Display $f_c \cong 6$ kHz. In addition to inward currents (approximately −100 mV), outward currents (approximately +50 mV) were also recorded in the presence of 2 mM ACh or 2 mM acetylthiocholine to relieve fast blockade by the agonist itself. This was not necessary in the presence of 20 mM choline because the increase in open-channel noise due to fast blockade was much lower (Grosman and Auerbach, 2000). Openings are downward deflections at −100 mV and upward deflections at +50 mV. The higher amplitude of the δS→T currents in the presence of 2 mM ACh at +50 mV, as compared with that of the wild type, is most likely due to the slower closing rate constant of the mutant.

netically most complex patches, accounts for the majority of openings). We found clear evidence that the opening rate constant increases as the membrane is hyperpolarized, in agreement with the results of Jackson (1986). We also found that the closing rate constant is not voltage dependent, as shown by Auerbach et al. (1996). Interestingly, the voltage dependence of the whole reaction is very close to that found for diliganded gating; i.e., ∼70-mV/*e*-fold (Neher and Steinbach, 1978; Auerbach et al., 1996). Thus, the unliganded and diliganded gating equilibria seem to have the same voltage dependence, as expected from a cyclic model with voltage-independent binding steps. The voltage dependences of the rate constants are, however, exactly opposite. Therefore, the relative position along the gating-reaction coordinate (i.e., closed-like versus open-like) of the structural elements that define voltage dependence, measured at the transition state, differs depending on whether the channel is bound or vacant (Grosman et al., 2000). We do not know whether these differences extend to other regions of the receptor. However, that the corresponding position of the transmitter binding site does not change with the number of bound ligands, is one of the assumptions of the use of linkage relationships to predict the rate constants of un- and monoliganded gating based on the (measured) rate constants of diliganded gating (Edelstein et al., 1996).

Coupling between Binding Sites and Pore

The results in Fig. 7 indicate that the binding-site mutations αY93F, αY190W, and αD200N impair unliganded gating. This can be interpreted as an indication that

TABLE VI

Effect of the δ12′S→T Mutation on Diliganded Gating

AChR	Agonist	Voltage	θ_2	*n*	θ_2 increase
Wild type	20 mM choline	−100 mV	0.054 ± 0.010	5	
12′ δS→T	20 mM choline	−100 mV	0.783 ± 0.059	7	14.5 ± 2.9
Wild type	2 mM acetylthiocholine	+50 mV	0.038 ± 0.003	3	
12′ δS→T	2 mM acetylthiocholine	+50 mV	0.496 ± 0.080	2	13.1 ± 2.3

Saturating concentrations of agonist were used to isolate gating from agonist-binding steps. In the presence of 20 mM choline or 2 mM acetylthiocholine, gating was modeled best by a C ↔ O reaction scheme. θ_2 values for each patch were estimated as the ratio of the opening rate constant and the closing rate (Grosman and Auerbach, 2000), and the values displayed here are the mean ± SEM for the indicated number of patches (*n*). The excess open-channel noise in the presence of 2 mM acetylthiocholine (due to fast block by the agonist) was conveniently reduced by depolarizing the patch to approximately +50 mV. Standard errors of the θ_2 increase were calculated using Eqs. 1 and 2 in the companion paper.

there is a conformational rearrangement around these binding-site residues during unliganded gating, whose manifestation at the pore is the opening–closing of the channel. This suggests that spontaneous openings do not arise from the autonomous activity of the M2 region.

This interpretation relies on the assumption that binding-site mutations can only cause local perturbations that do not reach the distant gate. We cannot rule out, however, the possibility that a local perturbation at the binding sites could propagate to the "autonomous gate" and affect its behavior. Nevertheless, crystallographic data of proteins shows that structural changes are usually greater near the sites of mutation and fall off rapidly with increasing distance (Skinner and Terwilliger, 1996). It could be argued that the AChR, being an allosteric protein, is "designed" to propagate local conformational changes from the binding sites to the pore region. For that reason, we tested three different binding-site positions, and the mutations were designed to be conservative in an attempt to minimize the magnitude of the local perturbation and the extent of its propagation. Therefore, it is likely that, regardless of local differences caused by the bound agonist (Kyte, 1995), the end points of the binding-site rearrangement during unliganded and diliganded gating are globally the same. This concept lends full support to the use of thermodynamic cycles to model the AChR's activity.

Control of the Isomerization Step by Binding-Site Residues

There are two ways a binding-site mutation can reduce θ_2: it can reduce the ligand-affinity difference between the open and closed states (the affinity ratio), or it can interfere with the low affinity $\rightarrow$ high affinity conformational change that accompanies channel opening (θ_0). Here, we showed that the decrease in θ_2 caused by the binding-site mutations αY93F, αY190W, and αD200N (Chen et al., 1995; Akk et al., 1996; Auerbach et al., 1996) is due, at least in part, to a decrease in θ_0 (Eq. 1). Thus, the use of spontaneously opening mutants as the background receptors on which other mutations are engineered constitutes a useful tool to identify binding-site residues that contribute to gating in forms other than by binding the agonist with different affinities in the open versus closed state. It is very likely that these residues, in addition to making contact with the ligand (at least in the case of αY93 and αY190), also participate in protein–protein interactions that change upon gating. This distinction between effects on θ_0 or the affinity ratio would have been difficult to make if the background receptor had been the wild-type channel.

It seems that the gating conformational change of AChRs is controlled in opposite directions by residues at the pore and the binding sites. With the exception of αG153S (Zhou et al., 1999a), we are not aware of binding-site mutations that increase spontaneous activity, nor are we aware of M2 mutations that substantially decrease it. Whether this reflects a fundamental aspect of the channel's design or just the paucity of mutational-analysis data remains to be ascertained.

Diliganded Activity

In the absence of a solid estimate of the number of channels per patch, we cannot estimate θ_0. As a consequence, it was impossible to determine directly whether the increase in θ_2 caused by the 12′ mutations arises exclusively from an equal increase in θ_0 or there is a contribution from a change in the affinity ratio as well. To solve this issue, we took an indirect approach reasoning that it is unlikely for a mutation that alters the affinity ratio of a receptor to do so to the same extent for different ligands. According to Eq. 1, it is clear that a mutation that increases θ_0 without affecting the affinity ratio causes the same increase in θ_2 for different agonists. Here we suggest that the reverse is also true: the same increase in θ_2 for different ligands can be taken as an (indirect) evidence that the mutation in question only affects θ_0. By comparing the responses of wild-type and δS$\rightarrow$T AChRs to two agonists (choline and acetylthiocholine), we concluded that the δS$\rightarrow$T mutation mainly affects θ_0.

As shown in Fig. 8, we cannot directly measure the effect of the δ12′ S$\rightarrow$T mutation on ACh-activated AChR gating. However, from the average increase in θ_2 for choline and acetylthiocholine ($\sim$13.8×), we can predict that θ_2 for ACh would be $\sim$380, which is 13.8× the θ_2 value for the wild-type AChR (calculated to be $\sim$27.5 at −100 mV, from data in Salamone et al., 1999). Further, based on the observation that opening (and closing) activation-free energies of δ12′ mutants are linearly correlated with the corresponding gating equilibrium free-energy changes, and that the slope of such relationship (Φ) is $\sim$0.3 for choline or acetylthiocholine (Grosman and Auerbach, 2000; Grosman et al., 2000), we can also predict the gating rate constants of ACh-bound receptors. This "linear free-energy relationship" (Leffler and Grunwald, 1963) implies that $\beta_{2mut}/\beta_{2wt} = (\theta_{2mut}/\theta_{2wt})^{\Phi}$ [and, therefore, $\alpha_{2mut}/\alpha_{2wt} = (\theta_{2mut}/\theta_{2wt})^{(\Phi - 1)}$]. Thus, the diliganded opening rate constant of δ12′ S$\rightarrow$T receptors should be $13.8^{0.3} \cong 2.2$ times that of wild-type AChRs, or $\sim$110,000 s^{-1}, and the closing rate constant should be $13.8^{-0.7} \cong 0.16$ times that of wild-type AChRs, or $\sim$300 s^{-1} (at −100 mV).

In the following paper, we make extensive use of choline as a slowly opening, low-efficacy agonist to investigate the effect of 12′ pore mutations on diliganded gating.

We thank Karen Lau for technical assistance.

This work was supported by grants from the National Institutes of Health to A. Auerbach and from the American Heart Association, New York State Affiliate, to C. Grosman.

Submitted: 24 September 1999
Revised: 3 March 2000
Accepted: 20 March 2000

REFERENCES

Akabas, M.H., C. Kaufmann, P. Archdeacon, and A. Karlin. 1994. Identification of acetylcholine receptor channel-lining residues in the entire M2 segment of the α subunit. *Neuron*. 13:919–927.

Akk, G., S. Sine, and A. Auerbach. 1996. Binding sites contribute unequally to the gating of mouse nicotinic αD200N acetylcholine receptors. *J. Physiol.* 496:185–196.

Auerbach, A., and C.J. Lingle. 1986. Heterogeneous kinetic properties of acetylcholine receptor channels in *Xenopus* myocytes. *J. Physiol.* 378:119–140.

Auerbach, A., W. Sigurdson, J. Chen, and G. Akk. 1996. Voltage dependence of mouse acetylcholine receptor gating: different charge movements in di-, mono- and unliganded receptors. *J. Physiol.* 494:155–170.

Ausubel, F.M., R. Brent, R.E. Kingston, D.D. Moore, J.G. Seidman, J.A. Smith, and K. Struhl. 1992. Short Protocols in Molecular Biology. John Wiley & Sons, New York, NY. 9.1.1–9.1.6.

Brehm, P., R. Kullberg, and F. Moody-Corbett. 1984. Properties of non-junctional acetylcholine receptor channels in innervated muscle of *Xenopus laevis*. *J. Physiol.* 350:631–648.

Chay, T.R. 1988. Kinetic modeling for the channel gating process from single channel patch clamp data. *J. Theor. Biol.* 132:449–468.

Chen, J., and A. Auerbach. 1998. A distinct contribution of the δ subunit to acetylcholine receptor channel activation revealed by mutations of the M2 segment. *Biophys. J.* 75:218–225.

Chen, Z.M., and M.M. White. 1999. The outer leucine ring is another determinant for AChR gating. *Biophys. J.* 76:A373. (Abstr.)

Chen, J., Y. Zhang, G. Akk, S. Sine, and A. Auerbach. 1995. Activation kinetics of recombinant mouse nicotinic acetylcholine receptors: mutations of α-subunit tyrosine 190 affect both binding and gating. *Biophys. J.* 69:849–859.

Croxen, R., C. Newland, D. Beeson, H. Oosterhuis, G. Chauplannaz, A. Vincent, and J. Newsom-Davis. 1997. Mutations in different functional domains of the human muscle acetylcholine receptor alpha subunit in patients with the slow-channel congenital myasthenic syndrome. *Hum. Mol. Genet.* 6:767–774.

Davies, P.A., M. Pistis, M.C. Hanna, J.A. Peters, J.J. Lambert, T.G. Hales, and E.F. Kirkness. 1999. The 5-HT3B subunit is a major determinant of serotonin-receptor function. *Nature.* 397:359–363.

Edelstein, S.J., and J.-P. Changeux. 1998. Allosteric transitions of the acetylcholine receptor. *Adv. Prot. Chem.* 51:121–184.

Edelstein, S.J., O. Schaad, E. Henry, D. Bertrand, and J.-P. Changeux. 1996. A kinetic mechanism for nicotinic acetylcholine receptors based on multiple allosteric transitions. *Biol. Cybern.* 75:361–379.

Eertmoed, A.L., and W.N. Green. 1999. Nicotinic receptor assembly requires multiple regions throughout the γ subunit. *J. Neurosci.* 19:6298–6308.

Engel, A.G., K. Ohno, M. Milone, H.-L. Wang, S. Nakano, C. Bouzat, J.N. Pruitt II, D.O. Hutchinson, J.M. Brengman, N. Bren, et al. 1996. New mutations in acetylcholine receptor subunit genes reveal heterogeneity in the slow-channel congenital myasthenic syndrome. *Hum. Mol. Genet.* 5:1217–1227.

Ferrer-Montiel, A.V., M.S. Montal, M. Díaz-Muñoz, and M. Montal. 1991. Agonist-independent activation of acetylcholine receptor channels by protein kinase A phosphorylation. *Proc. Natl. Acad. Sci. USA.* 88:10213–10217.

Gardner, P. 1990. Nucleotide sequence of the ϵ-subunit of the mouse muscle nicotinic receptor. *Nucleic Acids Res.* 18:6714.

Gibb, A.J., H. Kojima, J.A. Carr, and D. Colquhoun. 1990. Expression of cloned receptor subunits produces multiple receptors. *Proc. R. Soc. Lond. B Biol. Sci.* 242:108–112.

Grosman, C., and A. Auerbach. 2000. Asymmetric and independent contribution of M2 12′ residues to diliganded gating of acetylcholine receptor channels: a single-channel study with choline as the agonist. *J. Gen. Physiol.* 115:637–651.

Grosman, C., M. Zhou, and A. Auerbach. 2000. Mapping the conformational wave of acetylcholine receptor channel gating. *Nature.* 403:773–776.

Hamill, O.P., A. Marty, E. Neher, B. Sakmann, and F.J. Sigworth. 1981. Improved patch clamp technique for high resolution current recordings from cells and cell-free membrane patches. *Pflügers Arch.* 391:85–100.

Higuchi, R. 1990. Recombinant PCR. *In* PCR Protocols: A Guide to Methods and Applications. M.A. Innis, D.H. Gelfand, J.J. Sninsky, and T.J. White, editors. Academic Press, Inc., San Diego, CA. 177–183.

Horn, R., and K. Lange. 1983. Estimating kinetic constants from single channel data. *Biophys. J.* 43:207–223.

Jackson, M.B. 1984. Spontaneous openings of the acetylcholine receptor channel. *Proc. Natl. Acad. Sci. USA.* 81:3901–3904.

Jackson, M.B. 1986. Kinetics of unliganded acetylcholine receptor channel gating. *Biophys. J.* 49:663–672.

Jackson, M.B. 1989. Perfection of a synaptic receptor: kinetics and energetics of the acetylcholine receptor. *Proc. Natl. Acad. Sci. USA.* 86:2199–2203.

Jackson, M.B. 1994. Single channel currents in the nicotinic acetylcholine receptor: a direct demonstration of allosteric transitions. *Trends Biochem. Sci.* 19:396–398.

Jackson, M.B., K. Imoto, M. Mishina, T. Konno, S. Numa, and B. Sakmann. 1990. Spontaneous and agonist-induced openings of an acetylcholine receptor channel composed of α-, β- and δ-subunits. *Pflügers Arch.* 417:129–135.

Karlin, A., and M.H. Akabas. 1995. Toward a structural basis for the function of nicotinic acetylcholine receptors and their cousins. *Neuron*. 15:1231–1244.

Kearney, P.C., H. Zhang, W. Zhong, D.A. Dougherty, and H.A. Lester. 1996. Determinants of nicotinic receptor gating in natural and unnatural side chain structures at the M2 9′ position. *Neuron*. 17:1221–1229.

Korn, S.J., and R. Horn. 1991. Discrimination of kinetic models of ion channel gating. *In* Methods in Neurosciences. Vol. 4. Electrophysiology and Microinjection. P.M. Conn, editor. Academic Press, Inc., San Diego, CA. 428–456.

Kyte, J. 1995. Mechanism in Protein Chemistry. Garland Publishing, Inc., New York, NY. 461–519.

Lee, B.S., R.B. Gunn, and R.R. Kopito. 1991. Functional differences among nonerythroid anion exchangers expressed in a transfected human cell line. *J. Biol. Chem.* 266:11448–11454.

Leffler, J.E., and E. Grunwald. 1963. Rates and equilibria of organic reactions. John Wiley & Sons, New York, NY. 458 pp.

Machold, J., Y. Utkin, D. Kirsch, R. Kaufmann, V. Tsetlin, and F. Hucho. 1995a. Photolabeling reveals the proximity of the α-neurotoxin binding site to the M2 helix of the ion channel in the nicotinic acetylcholine receptor. *Proc. Natl. Acad. Sci. USA.* 92:7282–7286.

Machold, J., C. Weise, Y. Utkin, V. Tsetlin, and F. Hucho. 1995b. The handedness of the subunit arrangement of the nicotinic acetylcholine receptor from *Torpedo californica*. *Eur. J. Biochem.* 234: 427–430.

Magleby, K.L., and C.F. Stevens. 1972. The effect of voltage on the time course of end-plate currents. *J. Physiol.* 223:151–171.

Milone, M., H.-L. Wang, K. Ohno, T. Fukudome, J.N. Pruitt, N. Bren, S.M. Sine, and A.G. Engel. 1997. Slow-channel myasthenic

syndrome caused by enhanced activation, desensitization, and agonist binding affinity attributable to mutation in the M2 domain of the acetylcholine receptor α subunit. *J. Neurosci.* 17: 5651–5665.

Miyazawa, A., Y. Fujiyoshi, M. Stowell, and N. Unwin. 1999. Nicotinic acetylcholine receptor at 4.6 Å resolution: transverse tunnels in the channel wall. *J. Mol. Biol.* 288:765–786.

Monod, J., J. Wyman, and J.-P. Changeux, 1965. On the nature of allosteric transitions: a plausible model. *J. Mol. Biol.* 12:88–118.

Naranjo, D., and P. Brehm. 1993. Modal shifts in acetylcholine receptor channel gating confer subunit-dependent desensitization. *Science.* 260:1811–1814.

Neelands, T.R., J.L. Fisher, M. Bianchi, and R.L. Macdonald. 1999. Spontaneous and γ-aminobutyric acid (GABA)-activated $GABA_A$ receptor channels formed by ϵ subunit-containing isoforms. *Mol. Pharmacol.* 1:168–178.

Neher, E., and J.H. Steinbach. 1978. Local anesthetics transiently block currents through single acetylcholine-receptor channels. *J. Physiol.* 277:153–176.

Ohno, K., D.O. Hutchinson, M. Milone, J.M. Brengman, C. Bouzat, S.M. Sine, and A.G. Engel. 1995. Congenital myasthenic syndrome caused by prolonged acetylcholine receptor channel openings due to a mutation in the M2 domain of the ϵ subunit. *Proc. Natl. Acad. Sci. USA.* 92:758–762.

Qin, F., A. Auerbach, and F. Sachs. 1996. Estimating single-channel kinetic parameters from idealized patch-clamp data containing missed events. *Biophys. J.* 70:264–280.

Qin, F., A. Auerbach, and F. Sachs. 1997. Maximum likelihood estimation of aggregated Markov processes. *Proc. R. Soc. Lond. B Biol. Sci.* 264:375–383.

Rabiner, L.R., J.G. Wilpon, and B.H. Juang. 1986. A segmental-k-means training procedure for connected word recognition. *AT&T Tech. J.* 65:21–31.

Rothberg, B.S., and K.L. Magleby. 1998. Kinetic structure of large-conductance Ca^{2+}-activated K^+ channels suggests that the gating includes transitions through intermediate or secondary states. A mechanism for flickers. *J. Gen. Physiol.* 111:751–780.

Roux, B., and R. Sauvé. 1985. A general solution to the time interval omission problem applied to single channel analysis. *Biophys. J.* 48:149–158.

Salamone, F.N., M. Zhou, and A. Auerbach. 1999. A re-examination of adult mouse nicotinic acetylcholine receptor channel activation kinetics. *J. Physiol.* 516:315–330.

Schoepfer, R., W.G. Conroy, P. Whiting, M. Gore, and J. Lindstrom. 1990. Brain α-bungarotoxin binding protein cDNAs and MAbs reveal subtypes of this branch of the ligand-gated ion channel gene superfamily. *Neuron.* 5:35–48.

Sine, S.M. 1993. Molecular dissection of subunit interfaces in the acetylcholine receptor: identification of residues that determine curare selectivity. *Proc. Natl. Acad. Sci. USA.* 90:9436–9440.

Skinner, M.M., and T.C. Terwilliger. 1996. Potential use of additivity of mutational effects in simplifying protein engineering. *Proc. Natl. Acad. Sci. USA.* 93:10753–10757.

Swope, S.L., S.J. Moss, L.A. Raymond, and R.L. Huganir. 1999. Regulation of ligand-gated ion channels by protein phosphorylation. *Adv. Second Messenger Phosphoprotein Res.* 33:49–78.

Valenzuela, C.F., P. Weign, J. Yguerabide, and D.A. Johnson. 1994. Transverse distance between the membrane and the agonist binding sites on the *Torpedo* acetylcholine receptor: a fluorescence study. *Biophys. J.* 66:674–682.

Verrall, S., and Z.H. Hall. 1992. The N-terminal domains of acetylcholine receptor subunits contain recognition signals for the initial steps of receptor assembly. *Cell.* 68:23–31.

Villarroel, A., S. Herlitze, V. Witzemann, M. Koenen, and B. Sakmann. 1992. Asymmetry of the rat acetylcholine receptor subunits in the narrow region of the pore. *Proc. R. Soc. Lond. B Biol. Sci.* 249:317–324.

Wells, J.A. 1990. Additivity of mutational effects in proteins. *Biochemistry.* 37:8509–8517.

Zhang, H., and A. Karlin. 1998. Contribution of the β subunit M2 segment to the ion-conducting pathway of the acetylcholine receptor. *Biochemistry.* 37:7952–7964.

Zhou, M., A.G. Engel, and A. Auerbach. 1999a. Serum choline activates mutant acetylcholine receptors that cause slow channel congenital myasthenic syndromes. *Proc. Natl. Acad. Sci. USA.* 96: 10466–10471.

Zhou, M., C. Grosman, and A. Auerbach. 1999b. Single channel properties of the ϵ-less acetylcholine receptor channel. *Biophys. J.* 76:A371. (Abstr.)